Dielectric response in dilute lyotropic lamellar and sponge phases of a nonionic surfactant

Daisuke Mizuno, Takuji Nishino, Yasuyuki Kimura, and Reinosuke Hayakawa
Department of Applied Physics, Graduate School of Engineering, University of Tokyo, 7-3-1 Hongo, Bunkyo-ku, Tokyo 113-8656, Japan
(Received 18 June 2002; revised manuscript received 29 January 2003; published 27 June 2003)

We study the dielectric response in lyotropic lamellar and sponge phases made up of a binary mixture of a nonionic surfactant and water. A single relaxation is observed in both phases within the measured frequency range of $10–10^7$ Hz. This relaxation originates from the obstruction of electric current by insulating membranes. In the sponge phase, it depends on surfactant concentration and conductivity of solvent. The observed dependence is well-described quantitatively by the equivalent electric circuit of the sponge structure, including the effect of accumulation of ions at the interface between water and membrane. In the lamellar phase, there is little dependence of dielectric relaxation on surfactant concentration. This is presumably due to the fact that submicrometer-sized defects play a more important role in the electrical property in this phase than the lamellar structure in smaller length scales does. Our results offer some basic information to study more complicated systems composed of charged membranes in aqueous solution.

DOI: 10.1103/PhysRevE.67.061505 PACS number(s): 82.70.−y, 77.84.−s, 77.22.Gm, 87.16.Dg

I. INTRODUCTION

There are various kinds of structures made up of surfactant bilayers in solution [1]. One of these is vesicle phase where a bilayer forms a sphere enclosing solvent. Another one is lamellar L_α phase, which is a lyotropic smectic liquid crystalline phase composed of a stack of bilayers and solvents. Observations by electron microscope or conductivity measurements [2,3] suggest that L_α phase can be divided into subregions by their defect structure. The appearance of these subregions of L_α phase depends on the temperature and the concentration of cosurfactants. Since bilayers become more and more perforated, in general, as temperature or concentration of cosurfactants decreases, well-aligned lamellar appears only at higher temperatures or higher concentrations of cosurfactants in L_α phase. By further increasing temperature or adding cosurfactants, the well-aligned L_α phase turns into the isotropic phase made up of bilayers called sponge L_3 phase. In this phase, the bilayers form multiconnected or spongelike structure, where membranes divide the space into two and the volume occupied by hydrophobic tail is larger than that in L_α phase. This bicontinuous structure has been confirmed by the small-angle neutron scattering (SANS) [4–6], and direct observations by the freeze fracture electron microscope [2,3,7,8]. Although the sponge phase is an isotropic phase, a certain characteristic length is observed in the SANS spectra. This length corresponds approximately to the size of a sponge cell ξ that is estimated as $\xi = 3\delta/2\phi$ at the level of random mixing approximation [9], where ϕ is the volume fraction of surfactant and δ is the membrane thickness. Therefore, ξ is a little bit longer than the repeat distance of membranes, $d(=\delta/\phi)$, in L_α phase.

Strey *et al.* reported that these phases can also be identified by dc conductivity σ_{dc}, since the insulating membranes obstruct electric current [6]. They divided the origin of the reduction of dc conductivity into two. One is the trivial decrease of the concentration of low molecular ions due to the addition of insulating units, and the other is the obstruction caused by structured aggregates. The ratio of the reduced dc conductivity $\sigma' = \sigma_{dc}/(1-\phi)$ to the conductivity of pure brine σ_0, which is usually called obstruction factor, distinctly reflects the structure of aggregates in surfactant solution. The reported value of the obstruction factor in L_3 phase is about 0.6–0.7 [6,10,11], which suggests the topological similarity of the structure of disordered L_3 phase to that of regular bicontinuous cubic phase whose obstruction factor is about 2/3 [12]. It has also been reported that the obstruction factor in lamellar phase is usually larger than that in L_3 phase [3,6].

The measurement of dc conductivity is expected to give information on a characteristic structure of surfactant bilyers, while dynamic process of charge transfer can be studied by the dielectric spectroscopy. For example, in L_α phase of charged lipids, dispersive relaxation probably due to inhomogeneity in a sample has been frequently observed [13,14]. Even in the sponge phase of charged membranes, enormously large bimodal relaxations have been observed recently [10,11]. Cates *et al.* associated the high frequency mode with behavior on the scale of a single pore of the sponge, and the lower-frequency one with fluctuation in the in (out) order parameter that is the difference in the volume fraction of the two subspaces divided by membranes [15].

Dielectric response in a solution composed of charged membranes is important also from the biological point of view, since it is expected to give rich information on the processes, such as charge transfer or ion diffusion between and across biological membranes. But they have not yet been adequately addressed because complicated problems, including electrokinetic phenomena at surfaces of charged membranes and charge transfer in complex or inhomogeneous structures, must be handled simultaneously. In fact, it is suggested in Ref. [15] that the basic study of a simpler system composed of nonionic surfactants may give some important information to understand more complicated systems composed of charged membranes.

In this study, we measured dielectric response of a dilute aqueous solution of a nonionic surfactant, pentaethyleneglycol monododecylether ($C_{12}E_5$), in order to reduce the diffi-

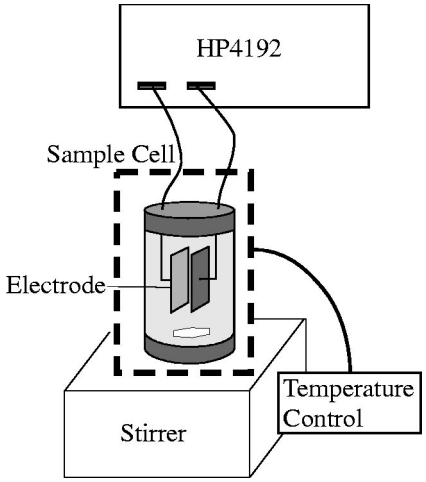

FIG. 1. Schematic illustration of the experimental setup.

culties mentioned above. A recent research [6] has revealed the phase diagrams and structures in each phase of our system, and L_3 and L_α phases are found to be stable even at very low concentration. Even in this rather simple system, its dynamic electrical properties have not been fully studied yet. For example, there may be two possible explanations for the hindrance mechanism of electrical current in L_3 and L_α phases. One is the so-called Maxwell-Wagner relaxation, which is caused by the inhomogeneity of electrical properties in a sample [13,14]. The other is the polarization induced by diffusion of low molecular ions [16,17] confined between membranes.

To distinguish between these mechanisms, we measured the dielectric response by changing the surfactant concentration and conductivity of a solvent. In both L_3 and L_α phases, only a single relaxation was observed in the frequency spectrum from ranging from 10 Hz to 10^7 Hz. The relationship between the structures in these phases and their dielectric responses is quantitatively discussed by their equivalent electric circuits. It is also found that the fluctuation of ionic concentration in aqueous phase plays an important role in the electrical property of our system, especially at low ionic strength.

II. EXPERIMENT

$C_{12}E_5$ (Wako) was diluted with aqueous solution of 0–0.02 wt% NaCl without further purification. The thickness of membrane δ of this sample determined by the small angle x-ray scattering is about 3 nm [18]. The volume fraction ϕ of $C_{12}E_5$ was varied from 1% to 5%. The dielectric response was repeatedly measured with temperature decreasing in a step of 0.3°C from the region above L_3 phase to below L_α phase. The schematic of the experimental configuration is shown in Fig. 1. The solution was stirred slowly to avoid macroscopic inhomogeneity and to prevent remaining quasiequilibrium for a long time. Without stirring, experimental results are not reproducible and no clear change in dielectric response can be observed at the transition point from L_3 to L_α phase. Samples were left for 2 min before measurement to attain equilibrium after the temperature is stabilized [19]. The complex impedance Z_s^* of the sample in a temperature-controlled cylindrical cell was measured by a LF impedance analyzer (HP4192A) in the frequency range from 10 Hz to 13 MHz. The parallel plate electrodes set in the cylindrical cell are made up of platinum coated with platinum black. The area S_0 and the distance d_0 between them are respectively, 4.5 cm^2 and 5 mm. The cell constant of the parallel plate electrodes was determined by measuring the capacitance of several liquids with known dielectric constant as 8.9 m^{-1}, and it is confirmed every time by using pure distilled water just before starting the measurement. Since the salt concentration is low compared to the previous experiments [6,10], contact resistance does not matter and electrode polarization is much smaller in this study. The measured impedance Z_s^* was analyzed by regarding the sample as a parallel circuit of frequency dependent capacitance $C_s(\omega)$ and conductance $G_s(\omega)$, where ω stands for frequency.

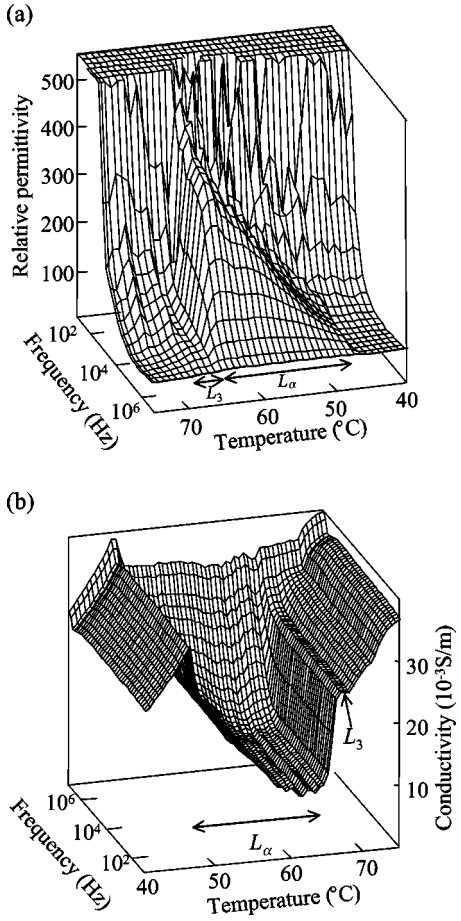

FIG. 2. Temperature dependence of frequency spectrum of (a) relative permittivity and (b) conductivity obtained for a sample with $\phi = 5\%$.

III. TEMPERATURE DEPENDENCE OF DIELECTRIC SPECTRUM IN L_3 AND L_α PHASES

In Fig. 2, we show the temperature dependence of frequency spectrum of relative permittivity and conductivity for

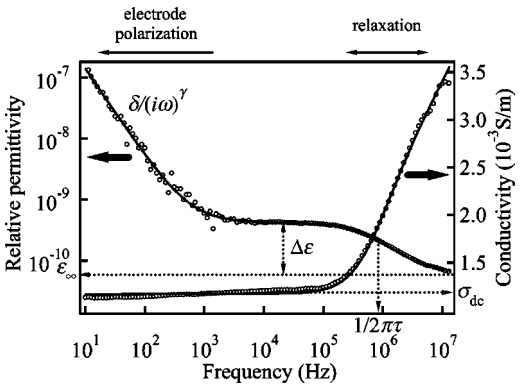

FIG. 3. Frequency dependence of the relative permittivity and conductivity for $\phi=5\%$ at 63.7 °C (L_α phase). The solid line is the best-fitted curve with Eq. (1).

the sample at $\phi=5\%$ in a three-dimensional plot. Both L_3 and L_α phases are clearly identified by the appearance of relaxation in these spectra. There is only one relaxation in the frequency spectrum at all temperatures in L_3 and L_α phases except the electrode polarization at low frequencies. These spectra are found to be well-fitted with the Cole-Cole type spectrum [20] given by

$$\varepsilon^*(\omega)=\frac{d_0}{S_0}\left\{C_s(\omega)+\frac{G_s(\omega)}{i\omega}\right\}$$
$$=\varepsilon_\infty+\frac{\Delta\varepsilon}{1+(i\omega\tau)^{\beta}}+\frac{\sigma_{\rm dc}}{i\omega}+\frac{\delta}{(i\omega)^{\gamma}}, \qquad (1)$$

where ε_∞ is the permittivity at high frequencies, $\Delta\varepsilon$ is the dielectric increment, τ is the relaxation time, and $\sigma_{\rm dc}$ is the dc conductivity. The exponent β denotes the broadness of relaxation and the last term in Eq. (1) denotes the electrode polarization, where the theoretically predicted value of γ is 1.5 [21]. Figure 3 shows the spectrum of permittivity and conductivity at $\phi=5\%$ in L_α phase (63.7 °C). The solid line is the best-fitted curve of Eq. (1). The best-fitted parameters are, respectively, $\Delta\varepsilon/\varepsilon_0=320$, $\varepsilon_\infty/\varepsilon_0=48.3$, $\tau=2.26\times10^{-7}$ s, $\sigma_{\rm dc}=9.57\times10^{-3}$ S/m, $\beta=0.845$, $\gamma=1.38$, and $\delta=6.41\times10^{-5}$. Since these parameters are necessary and sufficient to characterize the observed spectrum as explicitly shown in Fig. 3, they are insensitive to simultaneous variation in fitting so that the errors associated with the fits are small.

Temperature dependence of the obtained parameters $\sigma_{\rm dc}$, τ, and $\Delta\varepsilon$ are shown in Fig. 4. As mentioned before, $\sigma_{\rm dc}$ sensitively reflects the obstruction of electric current by insulating membranes in a solution. In this study, the conductivity of solvent σ_0 is roughly determined as the dotted line in Fig. 4, which is drawn by interpolating the data of $\sigma_{\rm dc}$ at 46 °C and 76 °C where obstruction seems to be very small. The value of σ_0 determined in such a way includes the contribution from impurity ions such as carbonate ions which are not negligible at the low ionic concentrations. The obstruction factor between 67.0 °C and 68.8 °C is about 2/3 so that this region is identified as L_3 phase. The factor is smaller at lower temperatures corresponding to L_α phase. The phase

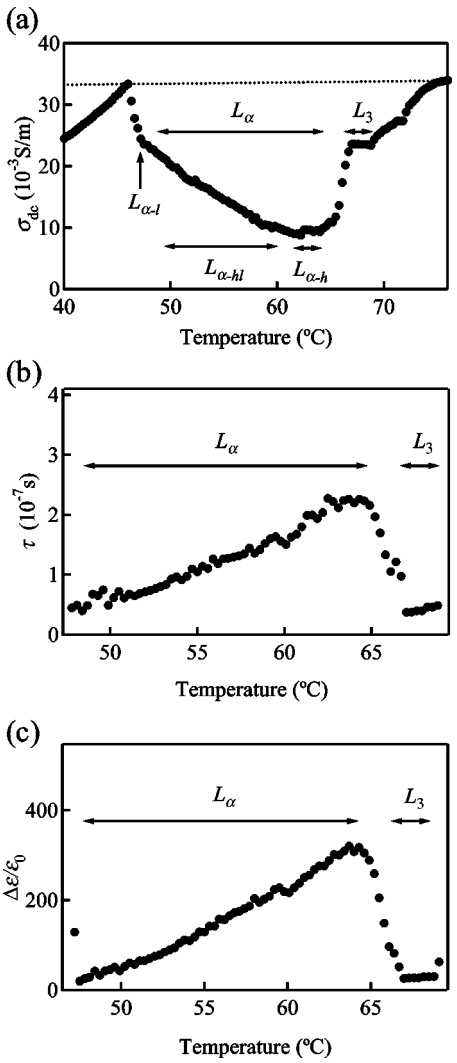

FIG. 4. Temperature dependence of the best-fitted parameters in Eq. (1) for $\phi=5\%$. (a) dc conductivity $\sigma_{\rm dc}$, (b) relaxation time τ, and (c) relative increment of permittivity $\Delta\varepsilon/\varepsilon_0$, where ε_0 is vacuum permittivity.

diagram of $C_{12}E_5$-water system identified from its dielectric response roughly agrees with the reported one [6] except the lower limit temperature of L_α phase, which is 55 °C in Ref. [6]. In the low-temperature region of L_α phase, experimental reproducibility is not sufficient and relaxation spectra tend to broaden. These observations indicate that it takes longer time to reach the equilibrium in the low-temperature region.

As shown in Fig. 4, the obtained relaxation parameters are almost constant in L_3 phase. On the other hand, the dielectric response in L_α phase largely depends on temperature. In L_α phase, τ and $\Delta\varepsilon$ are larger and $\sigma_{\rm dc}$ is smaller than those in L_3 phase, but these become closer to those in L_3 phase as temperature decreases. The observed temperature dependence is usually explained by the perforation of membranes at lower temperatures. The change of morphology in L_α phase is frequently observed by an electron microscope. Some researchers have divided L_α phase into three regions $L_{\alpha-h}$, $L_{\alpha-l}$, and $L_{\alpha-hl}$ [2,3]. Relatively well-aligned lamellas are observed only at the upper lamellar phase ($L_{\alpha-h}$).

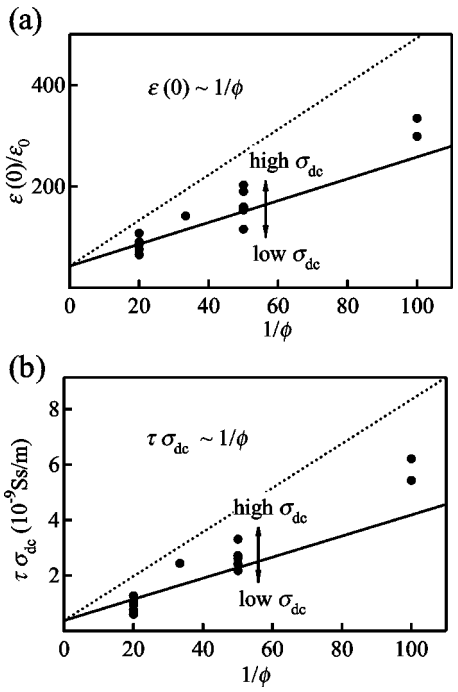

FIG. 5. Concentration ϕ dependence of (a) $\varepsilon(0)/\varepsilon_0$ and (b) $\tau\sigma_{\mathrm{dc}}$. Rough relationships between $\varepsilon(0) \propto 1/\phi$ and $\tau \propto 1/\phi\sigma_{\mathrm{dc}}$ are observed approximately. Solid lines are drawn by Eq. (4) using the measured permittivity of pure $C_{12}E_5$. The difference of the data points at the same volume fraction is its dc conductivity σ_{dc}. Dotted lines show the maximum values predicted for the high salt concentration.

The lower lamellar phase ($L_{\alpha-l}$) is composed of perforated vesicles and broken fragments of membranes, and $L_{\alpha-hl}$ is the mesophase of these two. In this study, we also divide L_α phase into three regions for convenience as shown in Fig. 4 according to the value of σ_{dc}. However, it should be noted that these subscripts are assigned only for convenience and we cannot assert that there should be actual phase transitions by our measurements.

IV. DIELECTRIC RESPONSE IN L_3 PHASE

The dependence of static permittivity $\varepsilon(0) \equiv \varepsilon_\infty + \Delta\varepsilon$ and of product of σ_{dc} and τ in L_3 phase on surfactant volume fraction ϕ are, respectively, shown in Figs. 5 (a) and 5(b). The relations $\varepsilon(0) \propto 1/\phi$ and $\sigma_{\mathrm{dc}}\tau \propto 1/\phi$, seem to be satisfied, and they are quite different from the relations $\Delta\varepsilon \propto \sigma_{dc}/\phi^2$ and $\tau \propto 1/\phi^2$, expected for the polarization induced by the diffusion of low molecular ions between membranes with separation $d \propto 1/\phi$. The observed dependence suggests that the dielectric relaxation in L_3 phase is the Maxwell-Wagner type. The Maxwell-Wagner effect is sometimes described by an equivalent electrical circuit composed of a register R and a capacitor C. In this study, the origin of respective parts of the equivalent circuit are distinctly identified. The insulating membrane can be regarded as a capacitor with capacitance C_2, and aqueous solvent can be regarded as a parallel circuit of a register $1/G_1$ and a capacitor C_1. Since the large fluctuation in L_3 phase is completely frozen at the observed relaxation frequency, the average structure of a unit cell of L_3 phase is electrically the same as that of cubic phase. The cubic phase is simply modeled as shown in Fig. 6(a), and its unit cell and its equivalent circuit are, respectively, shown in Figs. 6(b) and 6(c). The complex impedance Z^* or capacitance C^* of this equivalent circuit is calculated as

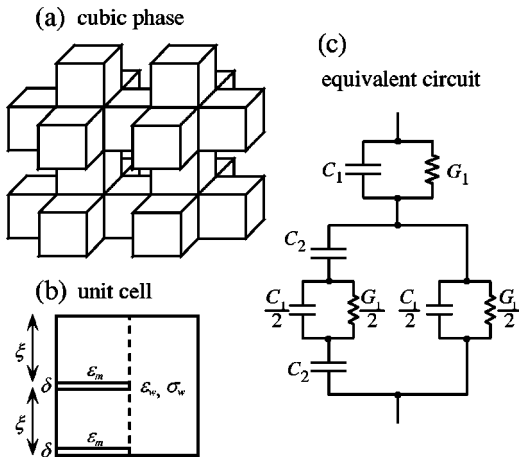

FIG. 6. (a) Cubic phase described by a cell model. The unit cell of this model (b) is almost the same as that of L_3 phase due to its topological similarity between L_3 and cubic phase. (c) The equivalent electric circuit of L_3 phase.

$$Z^* = \frac{i\omega(3C_1 + 4C_2) + 3G_1}{(i\omega C_1 + G_1)\{i\omega(C_1 + 2C_2) + G_1\}} = \frac{1}{i\omega C^*}. \quad (2)$$

By substituting $C_1 = \varepsilon_w S/\xi$, $G_1 = \sigma_w S/\xi$, $C_2 = \varepsilon_m S/2\delta$ (S is cross sectional area of the unit cell), and $\xi = 3\delta/2\phi$ into Eq. (2), the complex permittivity ε^* in L_3 phase is written as

$$\varepsilon^* = \frac{\varepsilon_w(3\varepsilon_m + 2\varepsilon_w\phi)}{3(\varepsilon_m + \varepsilon_w\phi)} + \frac{\varepsilon_m^2}{3(\varepsilon_m + \varepsilon_w\phi)\phi} \frac{1}{1 + i\omega(\varepsilon_m + \varepsilon_w\phi)/\phi\sigma_w} - \frac{2i\sigma_w}{3\omega}, \quad (3)$$

where ε_m and ε_w are the permittivities of bilayer membrane and solvent respectively. By comparing Eq. (1) with Eq. (3), we have

$$\varepsilon(0) \equiv \varepsilon_\infty + \Delta\varepsilon = \frac{2\varepsilon_w}{3} + \frac{\varepsilon_m}{3\phi}, \quad \sigma_{dc}\tau = \frac{2\varepsilon_w}{3} + \frac{2\varepsilon_m}{3\phi}. \quad (4)$$

The solid lines in Figs. 5(a) and 5(b) are drawn by using the measured value of $\varepsilon_m/\varepsilon_0 = 6.5$ and reported value of $\varepsilon_w/\varepsilon_0 = 65$ (at 65 °C), and they agree approximately with the experimental data. However, this model is too simplified to explain the conductivity dependence of $\varepsilon(0)/\varepsilon_0$ and $\tau\sigma_{dc}$ shown by the arrows in Fig. 5.

An applied electric field causes gradient in ionic concentration within a thin water layer adjacent to a membrane. Since back current induced by accumulation and exclusion of ions in this region cancels the total ionic flow, this thin layer acts as an insulator. The thickness of this layer is esti-

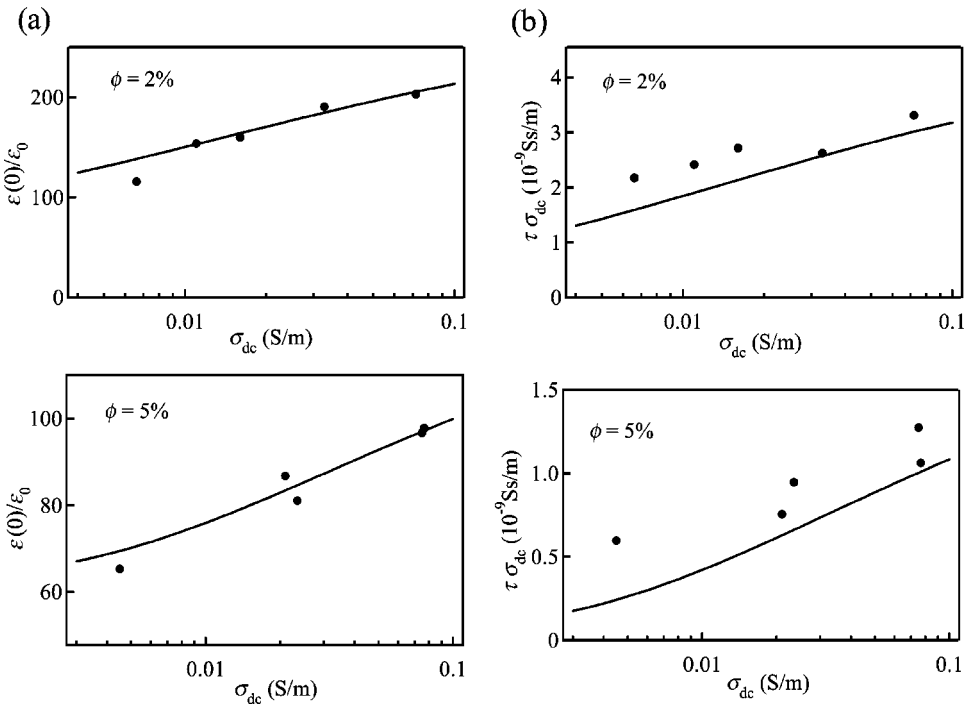

FIG. 7. dc conductivity σ_{dc} dependence of (a) $\varepsilon(0)/\varepsilon_0$ and (b) $\tau\sigma_{dc}$ at $\phi=2\%$ and 5%. Solid lines in (a) are the best-fitted curves with Eq. (6). Solid lines in (b) are the calculated curves by using the fitting parameters obtained from (a) and Eq. (7).

mated at the Debye length κ^{-1} and the total capacitance of the membrane, including the contribution from this thin water layer, is given by the series connection of two capacitors as $C_2=(2\delta/\varepsilon_m S+2/\varepsilon_w\kappa S)^{-1}$. More strictly, such an interfacial effect of ionic flow near the blocking surface is taken into account as an excess impedance connected with the capacitance of membrane in series. If the composition of valence of electrolytes is symmetric, the excess impedance Z_{ex} is written as [21–23]

$$Z_{ex}=\frac{2\beta D_i\kappa\tanh(\xi\sqrt{\kappa^2+i\omega/D_i}/2)}{i\omega S\sigma_w(1+i\omega\varepsilon_w/\sigma_w)\sqrt{1+i\omega/D_i\kappa^2}}. \tag{5}$$

Here, the parameter β is a constant of the order of unity, which will be determined afterwards, and D_i is the diffusion constant of low molecular ions. By replacing C_2 in Eq. (2) with $(1/C_2+i\omega Z_{ex})^{-1}$, we obtain

$$\varepsilon^*(\omega)=-\frac{A\{\varepsilon_w\kappa\delta(A/\sigma_w)^{1.5}(3i\varepsilon_m\omega+2\phi A)+2\beta\varepsilon_m\phi A\tanh[(3\delta\kappa/4\phi)\sqrt{A/\sigma_w}]\}}{3\omega\{\varepsilon_w\kappa\delta(-iA\phi+\varepsilon_m\omega)(A/\sigma_w)^{1.5}-i\beta\varepsilon_m\phi A\tanh[(3\delta\kappa/4\phi)\sqrt{A/\sigma_w}]\}}, \tag{6}$$

where we used the relation $D_i\kappa^2\sim\sigma_w/\varepsilon_w$ and $A\equiv\sigma_w+i\omega\varepsilon_w$. From this equation, we obtain

$$\varepsilon(0)=\frac{2\varepsilon_w}{3}+\frac{\varepsilon_w\varepsilon_m\delta}{3\phi[\varepsilon_w(\delta+\beta\varepsilon_m/\kappa)\tanh(3\kappa\delta/4\phi)]}, \tag{7}$$

and relaxation time τ is estimated as

$$\tau\sim\frac{\Delta\varepsilon}{\Delta\sigma}=\frac{\varepsilon_w(\varepsilon_m+\varepsilon_w\phi)[\kappa\delta-\beta\phi\tanh(3\kappa\delta/4\phi)]}{\sigma_w\phi[\varepsilon_w\kappa\delta+\beta\varepsilon_m\tanh(3\kappa\delta/4\phi)]}, \tag{8}$$

where $\Delta\sigma$ is the increment of conductivity. It is to be noted that $\Delta\varepsilon$ becomes zero in the case of $\kappa\xi\approx(\kappa\delta/\phi)\ll1$ (there is no Maxwell-Wagner relaxation), since the water phase totally acts as an insulator. In this case, we can determine β as 4/3 by Eq. (8). In the opposite case of $\kappa\xi\gg1$, where $\tanh(3\kappa\delta/4\phi)\sim1$, we have

$$\varepsilon(0)=\frac{2\varepsilon_w}{3}+\frac{\varepsilon_w\varepsilon_m\delta}{3\phi(\varepsilon_w\delta+\beta\varepsilon_m/\kappa)},$$

$$\tau=\frac{\Delta\varepsilon}{\Delta\sigma}=\frac{\varepsilon_w(\varepsilon_m+\varepsilon_w\phi)(\kappa\delta-\beta\phi)}{\sigma_w\phi(\varepsilon_w\kappa\delta+\beta\varepsilon_m)}. \tag{9}$$

The dependence of $\varepsilon(0)$ and $\tau\sigma_{dc}$ on dc conductivity σ_{dc} at $\phi=2\%$ and $\phi=5\%$ are, respectively shown in Figs. 7(a) and 7(b). The solid lines in Fig. 7(a) are the best-fitted curves with Eq. (7). For a fitting procedure, we used the reported value of $\varepsilon_w/\varepsilon_0=65$ and the linear relation between κ and $\sqrt{\sigma_w}$ as $\kappa=\alpha\sqrt{\sigma_w}$, and obtained $\alpha=6.6(\pm0.2)$

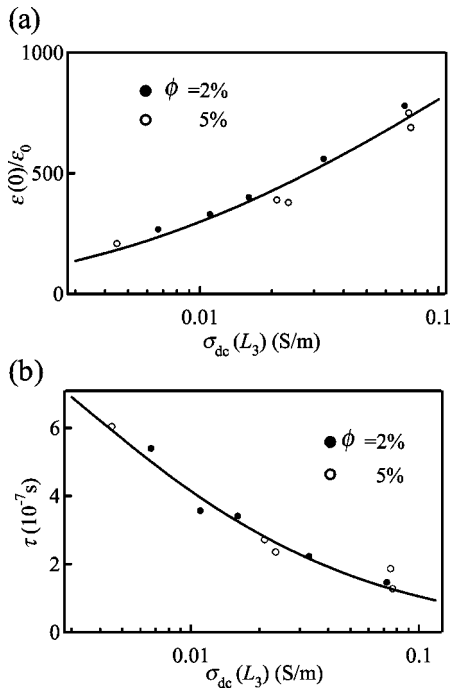

FIG. 8. Dielectric parameters $\varepsilon(0)/\varepsilon_0$ and τ in the higher temperature region of lamellar phase $L_{\alpha-h}$ plotted against the dc conductivity of sponge phase $\sigma_{\mathrm{dc}}(L_3)$. There are little dependences on surfactant concentration ϕ distinguished by the different markers. Solid lines in (a) and (b) are the best-fitted curves with Eq. (18).

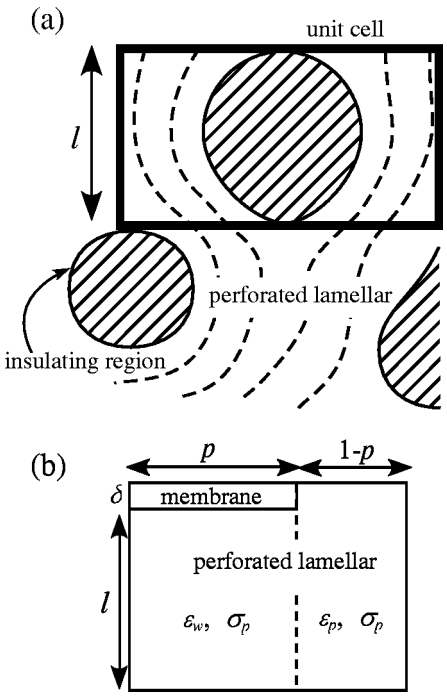

FIG. 9. (a) Schematic of lamellar phase composed of the perforated lamellar and vesiclelike region and (b) the unit cell supported by dielectric response.

$\times 10^8(\mathrm{S\,m})^{-1/2}$, $\varepsilon_m/\varepsilon_0=14(\pm 0.3)$ for $\phi=2\%$ and $\alpha=4.3(\pm 0.4)\times 10^8(\mathrm{S\,m})^{-1/2}$, $\varepsilon_m/\varepsilon_0=13(\pm 1)$ for $\phi=5\%$. Dotted lines in Figs. 5(a) and 5(b) are maximum values in the case of $\kappa\xi\gg 1$ drawn with Eq. (9)

Since typical value of D_i is about $1\sim 3\times 10^{-9}$ m^2 /s for the most kinds of low molecular ions, the obtained value of α is consistent with the theoretically estimated value of $\alpha=1/\sqrt{\varepsilon_w D_i}=0.7\sim 1.3\times 10^9(\mathrm{S\,m})^{-1/2}$. On the other hand, $\varepsilon_m/\varepsilon_0=13$–14 is larger than $\varepsilon_m/\varepsilon_0=6.5$ for pure $C_{12}E_5$. This increase of $\varepsilon_m/\varepsilon_0=6.5$ is probably due to the orientation of surfactant molecules in bilayers.

Solid lines in Fig. 7(b) are drawn by using Eq. (8) with the best-fitted parameters obtained for Fig. 7(a) and agree approximately with data. There are two reasons for the deviation at low ionic strength and high surfactant concentrations where the influence of ionic perturbation is crucial. One possible reason is that the distribution of ions assumed is slightly different from that in real system. The other reason is that we estimate the relaxation time in Eq. (8) from the ratio of the increment of permittivity to conductivity. Thus, the discrepancy becomes obvious when the neighboring insulating layers with κ^{-1} overlap one another.

Now we can explain the reasons why the induced polarization of ions dissolved in the solvent is not observed in our system. As shown in Eq. (4), the characteristic frequency of the Maxwell-Wagner relaxation is estimated as $\sigma_w/\varepsilon_w \sim D_i\kappa^2$. On the other hand, the characteristic frequency of the induced polarization is estimated as D_i/ξ^2. Therefore, when the Debye length κ^{-1} is smaller than the intermembrane distance ξ, the electric field applied to solvent between membranes considerably decreases at the frequencies below the Maxwell-Wagner relaxation and there might be no induced polarization. In the opposite case ($\kappa^{-1}>\xi$), there are no free ionic carriers in the solvent that acts as an insulator. In this situation, no induced polarization arises again.

Recently, Vinches *et al.* reported two relaxation modes in dielectric response of L_3 phase composed of charged membranes under very high salt concentration [10]. The observed high frequency mode was associated with the Maxwell-Wagner effect in Ref. [15], where the electrical double layer surrounding the charged membrane was regarded as a main component of the capacitance in series with the conductance of solvent. On the other hand, Vinches *et al.* reported that ε_∞ (permittivity at 15 MHz) is much larger than that of solvent and ε_∞ is scaled as $\varepsilon_\infty\sim 1/\phi$. The relaxation frequency of the corresponding Maxwell-Wagner effect becomes probably much higher than 15 MHz in their sample due to the extremely high concentration of added salt. Therefore, local electric field is almost parallel to the membranes below the frequency of the Maxwell-Wagner relaxation, and the transport of ions parallel to membrane may contribute to the reported giant relaxation modes.

V. DIELECTRIC RESPONSE IN L_α PHASE

To begin with, we discuss dielectric response in the $L_{\alpha-h}$ region where we can obtain reproducible data. Although a relaxation process in L_α phase is also expected to be the Maxwell-Wagner type, the observed behavior of relaxation

parameters in the $L_{\alpha-h}$ region is quite different from that in L_3 phase. There is little dependence on ϕ and all parameters mainly depend only on the conductivity of solvent σ_w, which is related to the dc conductivity of L_3 phase as $2/3\sigma_w$, as shown in Fig. 8. Such an independent nature on ϕ cannot be explained by an equivalent electric circuit to a periodic stacking of bilayers and solvents.

Since lamellar in our sample cell is not macroscopically oriented, there must be defects in a scale larger than the intermembrane distance. In fact, the vesiclelike structure or folded lamellar surrounded by perforated lamellar is frequently observed in freeze fracture electron micrographs [2,3]. These structures are electrically so inhomogeneous that there should be some regions where electric current hardly enter and other regions where the current can flow (presumably composed of perforated lamellar). Although the theoretical spectrum of dielectric response is already proposed for the concentrated vesicle dispersion [24], we use a simpler model to discuss the experimental results semiquantitatively. Since the outermost membranes of vesiclelike insulating region mainly hinders the electric current, we can assume that its inside is composed of perforated lamellar and is partially conductive. In this case, a unit cell for dielectric response is given as shown in Fig. 9(b). The size of a unit cell is not governed by the intermembrane distance d, but is determined by the effective size of the vesiclelike or folded structure l. The dielectric response of an equivalent circuit to this unit cell is given as

$$\varepsilon^*(\omega)=\frac{\varepsilon_p\{l\varepsilon_m+(1-p)\delta\varepsilon_p\}}{l\varepsilon_m+\delta\varepsilon_p}+\frac{(1-p)\sigma_p}{i\omega}+\frac{l^2p\varepsilon_m^2\sigma_p}{(l\varepsilon_m+\delta\varepsilon_p)\{\delta\sigma_p+i\omega(l\varepsilon_m+\delta\varepsilon_p)\}}, \quad (10)$$

where ε_p and σ_p are the permittivity and conductivity of perforated lamellar, respectively, and p is the effective ratio of the vesiclelike region.

Electric displacement $\boldsymbol{D}$ in the smectic phase is locally written as $\boldsymbol{D}=\tilde{\boldsymbol{\varepsilon}}_p\boldsymbol{E}=\varepsilon_\parallel\boldsymbol{E}_\parallel+\varepsilon_\perp\boldsymbol{E}_\perp$, where $\boldsymbol{E}_\perp$ and $\boldsymbol{E}_\parallel$ denote the components of the electric field $\boldsymbol{E}$ normal and parallel to the membrane, respectively, and $\varepsilon_\perp$, $\varepsilon_\parallel$ are simply written as

$$\varepsilon_\perp=\frac{d\varepsilon_m(\sigma_w+i\omega\varepsilon_w)}{\sigma_w\delta+i\omega(d\varepsilon_m+\delta\varepsilon_w)}, \quad \varepsilon_\parallel=\varepsilon_w+\frac{\sigma_w}{i\omega}. \quad (11)$$

The angle-averaged permittivity $\bar{\varepsilon}$ of perforated lamellar, where membranes are fragmented and not macroscopically oriented, is simply given by $\bar{\varepsilon}=\frac{1}{3}(\varepsilon_\perp+2\varepsilon_\parallel)$. It should be noted that $\bar{\varepsilon}$ will give the same expression as Eq. (3) obtained for L_3 phase. Therefore, Eq. (3) is available to the complex permittivity of perforated lamellar $\varepsilon_p^*=\varepsilon_p+\sigma_p/i\omega$. However, the real part of ε_p^* is not so important in Eq. (10), except in the case of $p\ll1$, because of the relation $l\gg\delta$. Therefore, we approximate ε_p of insulating region to ε_w. Finally, the dielectric response of the equivalent circuit to this unit cell, including the effect of ionic flow, is given as

$$\varepsilon^*(\omega)=\frac{\varepsilon_w\kappa\sqrt{A/\sigma_w}[pl\varepsilon_mB\omega-i(1-p)CD]-2i(1-p)\varepsilon_m\sigma_wC}{\omega(2\varepsilon_m\sigma_w+\kappa\varepsilon_wD\sqrt{A/\sigma_w})}, \quad (12)$$

where $A=\sigma_w+i\varepsilon_w\omega$, $B=\sigma_p+i\varepsilon_w\omega$, $C=\sigma_p+i\varepsilon_p\omega$, and $D=\delta B+i\omega l\varepsilon_m$. In Eq. (12), the same excess impedance as that in Eq. (5) is used except for exchanging ξ with l, since the thin perturbation layer is almost always composed of aqueous phase, and it is assumed that $\tanh(l\kappa\sqrt{1+i\omega\varepsilon_w/\sigma_w}/2)\sim1$.

Equation (12) is also approximated by the Cole-Cole function if the plausible value is substituted into each parameter. When it is approximated as $\varepsilon_p(\infty)\sim\varepsilon_w$ and $\sigma_p(\infty)\sim\sigma_w$, we have

$$\varepsilon(0)=(1-p)\varepsilon_p(0)+\frac{p\varepsilon_m\varepsilon_w\kappa l}{3\varepsilon_m+\varepsilon_w\kappa\delta}, \quad (13)$$

$$\Delta\sigma=\frac{1}{3}(1-p)\sigma_w+\frac{l^2\varepsilon_m^2p\sigma_w}{(l\varepsilon_m+\delta\varepsilon_w)^2}, \quad (14)$$

$$\Delta\varepsilon=(1-p)[\varepsilon_p(0)-\varepsilon_w]-\frac{l\varepsilon_m\varepsilon_wp}{l\varepsilon_m+\delta\varepsilon_w}+\frac{l\varepsilon_m\varepsilon_w\kappa p}{3\varepsilon_m+\varepsilon_w\kappa\delta}, \quad (15)$$

$$\sigma_{\mathrm{dc}}=(1-p)\sigma_p(0)=\tfrac{2}{3}(1-p)\sigma_w, \quad (16)$$

$$\tau\sim\frac{\Delta\varepsilon}{\Delta\sigma}. \quad (17)$$

In the case of $l\gg\kappa^{-1},\delta$, Eqs. (13) and (17) are rewritten as

$$\varepsilon(0)\sim\frac{p\varepsilon_m\varepsilon_w\kappa l}{3\varepsilon_m+\varepsilon_w\kappa\delta}, \quad \tau\sim\frac{3p\varepsilon_m\varepsilon_w\kappa l}{(1+2p)\sigma_w(3\varepsilon_m+\varepsilon_w\kappa\delta)}. \quad (18)$$

As shown in Eq. (16), p is directly obtained from the measured dc conductivity in L_α phase and from σ_w, which can be estimated from the dc conductivity in L_3 phase, σ_{dc} (L_3), as $\sigma_w=3\sigma_{\mathrm{dc}}(L_3)/2$. In Fig. 10, p in the $L_{\alpha-h}$ region is plotted against σ_{dc} (L_3). The ratio p in the $L_{\alpha-h}$ does not show clear dependence on ϕ. It is also expected that the effective size of insulating region l is mainly determined by the prop-

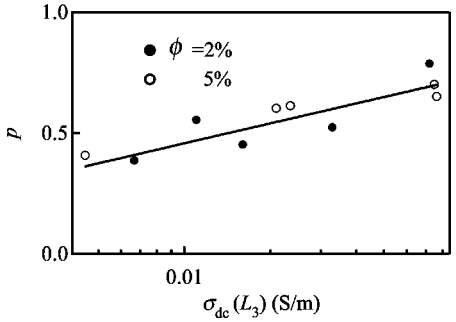

FIG. 10. Effective ratio of the insulating region p plotted against $\sigma_{\mathrm{dc}}(L_3)$. There seems to be little dependence on surfactant concentration ϕ and the solid line shows an experimentally obtained relationship.

erty of a single membrane. Probably, the independent nature of these values on ϕ makes dielectric response in the $L_{\alpha-h}$ region insensitive to ϕ. The approximate relation $p=0.12\ \ln(\sigma_{\mathrm{dc}})+1.0$ is experimentally found as shown by a solid line in Fig. 10. By using this relation, the relaxation time τ and static relative permittivity $\varepsilon(0)$ in the $L_{\alpha-h}$ region are, respectively, fitted with Eq. (18) as shown by the solid line in Figs. 8(a) and 8(b). In the fitting procedure, we used the previously obtained value of $\varepsilon_m/\varepsilon_0 \sim 13.5$ and the reported value of $\varepsilon_w/\varepsilon_0 \sim 65$. The best-fitted values of parameters are $\alpha=\kappa/\sqrt{\sigma_w}=1.2(\pm 0.3)\times 10^9\ (\mathrm{S\,m})^{-1/2}$ and $l=3.6(\pm 0.5)\times 10^{-7}$ m for the data shown in Fig. 8(a) and $\alpha=5.8(\pm 2.4)\times 10^8\ (\mathrm{S\,m})^{-1/2}$ and $l=8.6(\pm 2.4)\times 10^{-7}$ m for Fig. 8(b). Although Eq. (18) succeeds to explain the qualitative dependence of relaxation parameters on σ_{dc}, it may be too simplistic for quantitative discussion especially in the case of low ionic concentrations.

Therefore, we directly fitted the measured relaxation time τ and the static relative permittivity in the $L_{\alpha-h}$ region with Eqs. (17) and (13) respectively. In the fitting procedure, the measured values of the static permittivity and the dc conductivity in L_3 phase are used for $\varepsilon_p(0)$ and $2\sigma_w/3$. The discrete values shown as circles in Fig. 10 are used for p. The best-fitted values of parameters are $\alpha=5.2(\pm 2.2)\times 10^8\ (\mathrm{S\,m})^{-1/2}$ and $l=4.8(\pm 1.2)\times 10^{-7}$ m for $\varepsilon(0)$, and $\alpha=8.3(\pm 3.7)\times 10^8\ (\mathrm{S\,m})^{-1/2}$ and $l=6.6(\pm 2.1)\times 10^{-7}$ m for τ, which roughly agree with each other and verify our analysis. In Figs. 11(a) and 11(b), the comparison between experimental data and theory are shown by the $\sigma_{\mathrm{dc}}(L_3)$ dependence of the values given on the left-hand side of the following equations, which are rewrites of Eqs. (14) and (17),

$$\frac{\varepsilon(0)-(1-p)\varepsilon_p(0)}{p}=\frac{\varepsilon_m\varepsilon_w\kappa l}{3\varepsilon_m+\varepsilon_w\kappa\delta}, \tag{19}$$

$$\tau\left\{\frac{(1-p)}{3p}+\frac{\varepsilon_m^2 l^2}{(\varepsilon_m l+\varepsilon_w\delta)^2}\right\}-\frac{(1-p)(\varepsilon_p(0)-\varepsilon_w)}{p\sigma_w} =\frac{\varepsilon_m\varepsilon_w l}{\sigma_w}\left\{\frac{\kappa}{3\varepsilon_m+\varepsilon_w\kappa\delta}-\frac{1}{\varepsilon_m l+\varepsilon_w\delta}\right\}. \tag{20}$$

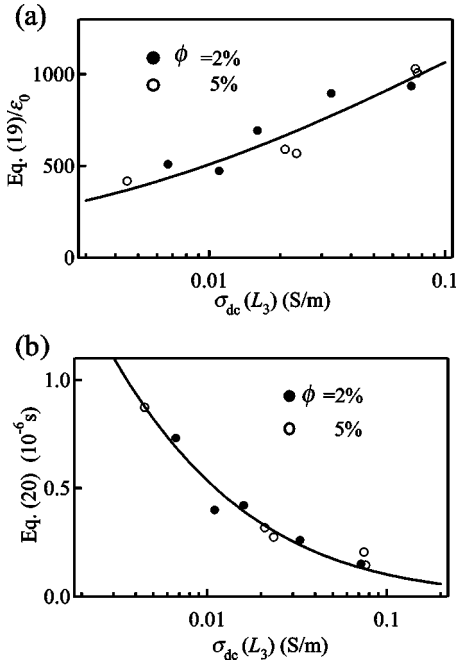

FIG. 11. $\sigma_{\mathrm{dc}}(L_3)$ dependence of the values given as the left-hand side of Eqs. (19) and (20) in the higher temperature region of lamellar phase $L_{\alpha-h}$. Solid lines are drawn with the right-hand side of the respective equations.

The obtained value of l is found to be comparable to the persistence length estimated from the bending modulus $k_c=1.3k_BT$ [6] of a single membrane as $\delta\exp(4\pi k_c/3k_BT)\sim 700$ nm.

Equation (12) explains the temperature dependence of dielectric response in the lamellar phase by assuming the plausible behavior of p and l. The parameter p becomes smaller as temperature decreases due to the perforation of lamellar. If fully perforated lamellar ($p=0$) appears in the $L_{\alpha-l}$ region, which is the lowest temperature part of L_α phase, the dielectric response in this region is indistinguishable from that in L_3 phase as explained before. In fact, the observed spectra in the $L_{\alpha-l}$ region and L_3 phase for $\phi=5\%$ are quite similar to each other as shown in Fig. 12.

Temperature dependence of p determined by $1-\sigma_{\mathrm{dc}}/\sigma_{dc}(L_3)$ for $\phi=5\%$ is drawn as a solid line in Fig. 13.

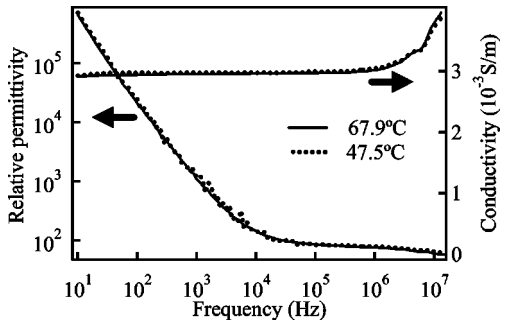

FIG. 12. Comparison of dielectric spectrum in L_3 phase (solid line) with that in L_α phase at the lower limit temperature (dotted line).

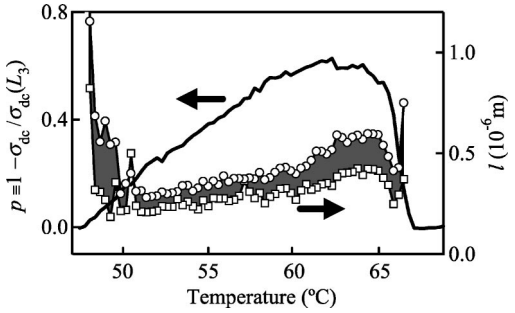

FIG. 13. Temperature dependence of l (right axis) obtained from $\Delta\varepsilon/\varepsilon_0$ with Eq. (13) (squares) and from τ with Eq. (17) (circles) in $\phi=5\%$. The ratio p determined by $1-\sigma_{dc}/\sigma_{dc}(L_3)$ is also shown (left axis).

Temperature dependence of l obtained from Eqs. (13) and (17) combined with the best-fitted values of τ and $\Delta\varepsilon/\varepsilon_0$ shown in Figs. 4(b) and 4(c) are, respectively, drawn as the empty squares and empty circles in Fig. 13. In the evaluation process, the previously obtained values of $\alpha=5.3\times10^8\ (\mathrm{S\,m})^{-1/2}$ and $\alpha=8.3\times10^8\ (\mathrm{S\,m})^{-1/2}$ are, respectively, used for Eqs. (13) and (17). The calculated values of l both show the similar dependence on temperature. It seems that effective size of a vesiclelike insulating region decreases as the membrane becomes perforated. This change of structure is usually explained by the packing of surfactants in a membrane. As the temperature decreases, volume occupied by the hydrophobic tails of surfactants in a membrane becomes smaller, which causes the negative Gaussian curvature modulus [25]. Smaller vesiclelike folded structure may be thus favored at lower temperature region in L_α phase.

VI. CONCLUSION

In conclusion, we measured the dielectric response in lyotropic lamellar and sponge phases made up of a nonionic surfactant and water, and observed a Maxwell-Wagner relaxation influenced by the charge accumulation at the interface between membrane and water. In the sponge phase, the dependence of relaxation on both surfactant and ionic concentrations reflects the characteristic structure of sponge phase. On the other hand, in the lamellar phase, its smectic structure has little influence on its electrical property, but we found micrometer-sized vesiclelike defects and perforation of membranes play more important role in its electrical property. This makes the dependence of electrical property on surfactant concentration obscure. Our results may give some basic information for understanding the dynamic electrical properties of other complex systems composed of lipid membranes. For example, inhomogeneity of structure or ionic activity in condensed gel-like lamellar and biological tissues composed of membranes causes another type of relaxation (so-called α dispersion). Charge transfer and ion diffusion processes between and across such membranes are also pivotal in a variety of biophysical processes. In these rather slower processes, local electric field strongly influenced by the Maxwell-Wagner effect, which is modified by charge fluctuation, may play an important role [26].

ACKNOWLEDGMENTS

This work was supported by a Grant-in-Aid for Scientific Research from the Japan Society for the Promotion of Science and the Ministry of Education, Culture, Sports, Science and Technology of Japan. D.M. was also supported by a grant from the Japan Society for the Promotion of Science.

[1] *Micells, Membranes, Microemulsions and Monolayers*, edited by W. M. Gelbart, A. Ben-Shaul, and D. Roux (Springer-Verlag, Berlin, 1994).
[2] T. Imae, T. Iwamoto, G. Platz, and C. Thunig, Colloid Polym. Sci. **269**, 727 (1991).
[3] H. Hoffmann, U. Munkert, C. Thunig, and M. Valiente, J. Colloid Interface Sci. **163**, 217 (1994).
[4] D. Gauzeau, A.M. Bellocq, D. Roux, and T. Zemb, Europhys. Lett. **9**, 447 (1989).
[5] G. Porte, J. Marignan, P. Bassereau, and R. May, J. Phys. (Paris) **49**, 511 (1989).
[6] R. Strey, R. Schomäcker, D. Roux, F. Nallet, and U. Olsson, J. Chem. Soc., Faraday Trans. **86**, 2253 (1990).
[7] H. Hoffmann, C. Thunig, U. Munkert, H.W. Meyer, and W. Richter, Langmuir **8**, 2629 (1992).
[8] R. Strey, W. Jahn, G. Porte, and P. Bassereau, Langmuir **6**, 1635 (1990).
[9] M.E. Cates, D. Roux, D. Andelmann, S. Milner, and S. Safran, Europhys. Lett. **5**, 733 (1988).
[10] C. Vinches, C. Coulon, and D. Roux, J. Phys. II **4**, 1165 (1994).
[11] I. Alibert, C. Coulon, A.M. Bellocq, and T. Gulik-Krzywicki, Europhys. Lett. **39**, 563 (1997).
[12] D.M. Anderson and H. Wennerström, J. Phys. Chem. **94**, 8683 (1990).
[13] R. He and D.Q.M. Craig, J. Phys. Chem. B **102**, 1781 (1998).
[14] J. Cooper and R.M. Hill, J. Colloid Interface Sci. **180**, 27 (1996).
[15] M.E. Cates, P. Schoot, and C.Y.D. Lu, Europhys. Lett. **29**, 669 (1995).
[16] G. Schwartz, J. Phys. Chem. **66**, 2636 (1962).
[17] M. Fixman, J. Chem. Phys. **72**, 5177 (1980).
[18] E. Freyssingeas, F. Nallet, and D. Roux, Langmuir **12**, 6028 (1996).
[19] Equilibration in this condition is fully confirmed at L_3 phase and at high temperature region of L_α phase, $L_{\alpha-h}$. We observed no change between the data measured in this condition and that after keeping at rest for sufficiently long time.
[20] K.S. Cole and R.H. Cole, J. Chem. Phys. **9**, 341 (1941).
[21] P.A. Cirkel, J.P.M. van der Ploeg, and G.J.M. Koper, Physica A **235**, 269 (1997).

[22] E.M. Trukhan, Sov. Phys. Solid State **4**, 2560 (1963).
[23] T.S. Sørensen and V. Campan, J. Chem. Soc., Faraday Trans. **91**, 4235 (1995).
[24] H. Zhang, K. Sekine, T. Hanai, and N. Koizumi, Colloid Polym. Sci. **261**, 381 (1983).
[25] G. Porte, J. Appell, P. Bassereau, and J. Marignan, J. Phys. (France) **50**, 1335 (1989).
[26] D. Mizuno, Y. Kimura, and R. Hayakawa, Phys. Rev. Lett. **87**, 088104 (2001).